Size-Dependent Grain-Boundary Structure with Improved Conductive and Mechanical Stabilities in Sub-10-nm Gold Crystals

Chunyang Wang,[1,2] Kui Du,[1,*] Kepeng Song,[1] Xinglong Ye,[1] Lu Qi,[1] Suyun He,[1] Daiming Tang,[1] Ning Lu,[3] Haijun Jin,[1] Feng Li,[1] and Hengqiang Ye[1]

[1]*Shenyang National Laboratory for Materials Science, Institute of Metal Research, Chinese Academy of Sciences, Shenyang 110016, China*

[2]*University of Chinese Academy of Sciences, Beijing 100049, China*

[3]*Department of Materials Science and Engineering, Case Western Reserve University, Cleveland, Ohio 44106, USA*

(Received 13 August 2017; revised manuscript received 16 December 2017; published 4 May 2018)

Low-angle grain boundaries generally exist in the form of dislocation arrays, while high-angle grain boundaries (misorientation angle >15°) exist in the form of structural units in bulk metals. Here, through *in situ* atomic resolution aberration corrected electron microscopy observations, we report size-dependent grain-boundary structures improving both stabilities of electrical conductivity and mechanical properties in sub-10-nm-sized gold crystals. With the diameter of a nanocrystal decreasing below 10 nm, the high-angle grain boundary in the crystal exists as an array of dislocations. This size effect may be of importance to a new generation of interconnects applications.

DOI: 10.1103/PhysRevLett.120.186102

Metallic nanowires can be widely used as interconnects [1,2], electrodes [3–5], and nanoantennas [6] in nano- or molecular devices. With silicon transistors rapidly approaching dimensions down to the sub-10-nm range [7], the performance of interconnects has become one of the major limiting factors in nanodevices [8,9]. Since both high electrical conductivity and good mechanical properties are required for conducting materials [10], gold nanowires become a promising candidate for interconnects in nano- or molecular devices [11]. Hence, submicron metallic pillars or nanorods or nanowires have been investigated by tension [12–17], compression [18–22], and bending tests [23,24]. While grain boundaries (GBs) in nanorods or nanowires have great influence on their performance [25], it seems unlikely to completely avoid GB formation in nanorods or nanowires during manufacturing or use, especially for applications such as interconnects in flexible electronic devices. In particular, as the diameter of a nanorod or nanowire goes below 10 nm, the remarkable interaction between surfaces and GBs will have much more significant influence on GB structures and behaviors different from that in bulk metals or alloys [26–32]. For instance, in bulk materials, GBs are usually categorized as low-angle GBs and high-angle GBs depending on their misorientation angles, while low-angle GBs (with misorientation angles less than ∼15°) are usually considered and described by dislocations [33] but high-angle GBs are not [34]. Whether this is significantly modified in nanorods has not been explored theoretically at present. Moreover, different structures of GBs [35] could have different effects on the electrical properties of metals. Generally, high-angle GBs [36,37] should correspond to much higher electrical resistivity than low-angle GBs [35,38–40]. For instance, Shao *et al.* [41] reported that the electrical conductivity of an alloy film deteriorated badly when it was turned from single crystal into polycrystal with high-angle GBs in dominance. For metal nanorods or nanowires with dimensions down to sub-10-nm, the size effects on GB structures and corresponding influences on electrical conductivity and mechanical properties of nanorods or nanowires remain obscure.

Here, we present *in situ* electrical conductivity measurements and deformation tests on gold nanorods with aberration corrected high-resolution transmission electron microscopy (AC-HRTEM). When the diameter of a nanorod is reduced to several nanometers, a high-angle GB can exist as dislocation arrays, and the smaller the diameter, the more stable for the high-angle GB existing as a dislocation type rather than a structural unit type. When the size of a nanorod decreases to 2 nm, a GB with a misorientation angle up to 28.6° exists as an array of dislocations. By using a scanning-tunneling-microscopy- (STM) TEM probe system, the electrical resistance of a single structural-unit-type GB in gold nanorods has been measured. Since dislocation-type GBs have much less electrical resistivity than structural-unit-type ones, the stability of electrical conductivity of nanorods with sub-10-nm diameters would be improved by forming dislocation-type GBs rather than structural-unit-type GBs.

The nanoporous gold (NPG) specimens were made by an electrochemical dealloying method [42,43] and nanorods (see Fig. S1 in the Supplemental Material [44]) were provided by Mogreat Materials Co. *In situ* deformation and electrical experiments were conducted with a FEI Titan G2 cubed 60-300 double aberration corrected electron microscope and a FEI F20 electron microscope. *In situ*

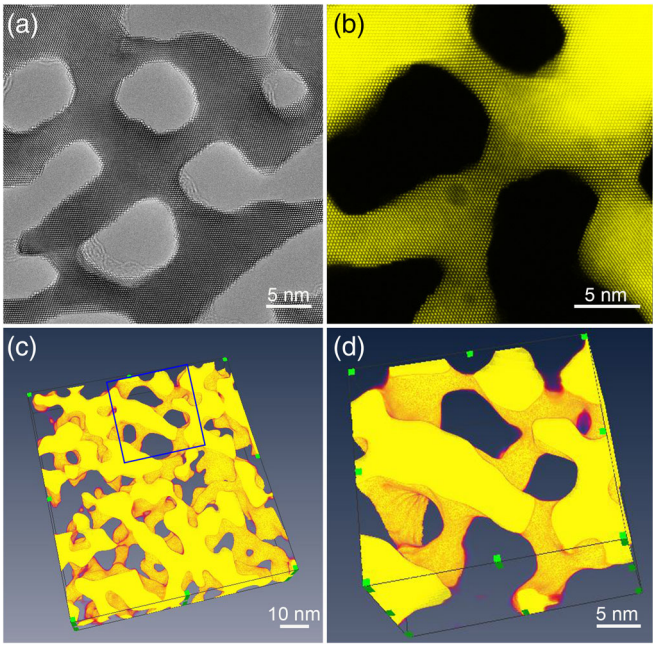

FIG. 1. Structure of a NPG specimen. (a) AC-HRTEM image of NPG. (b) Aberration corrected HAADF STEM image of NPG. (c) Surface render of NPG by electron tomography. (d) Enlarged image of the blue-box region in (c).

electrical measurements were conducted in a Nanofactory STM-TEM probe system. Figures 1(a) and 1(b) show AC-HRTEM and aberration corrected high-angle annular dark field scanning transmission electron microscopy (HAADF STEM) images of NPG. Figures 1(c) and 1(d) show the surface render of NPG by electron tomography (see Video M1 [44]). The NPG is comprised of nanorods with the diameters ranging from one to tens of nanometers and the lengths from several to tens of nanometers.

Both dislocation-type and structural-unit-type GBs were observed in deformed gold nanorods. Figure 2(a) shows a dislocation-type GB (DGB) in a gold nanorod. The misorientation angle of the GB is ~14.5°, which is in the low-angle GB regime but close to the generally believed critical angle of ~15° between low-angle and high-angle GBs in bulk metals [33]. Figure 2(b) clearly shows that the DGB is comprised of an array of dislocations. As the GB is asymmetrical, a small stress is induced by the asymmetrical nature of the GB while the strain around the GB is dominated by the dislocations accommodating the misorientation angle according to the equations in Ref. [33] (for details, see Sec. S2 of Ref. [44]) The characteristic angle φ between two basic vectors u (or u') and v (or v') is employed to define the crystal lattices across the DGB, while the angle φ is measured by the LADIA program [59–61], and the distribution of φ is shown in Fig. 2(c). Line profiles [Fig. 2(d)] were extracted from the analysis results for three (111) planes across the DGB. The result shows a continuously smooth change of φ across the DGB, which indicates the elastic strain induced by the GB dislocations. Similar elastic strain was also measured from the HAADF STEM image of a DGB (Fig. S3 of Ref. [44]).

Figures 2(e) and 2(f) show a $\Sigma 11(113)$ structural-unit-type GB (SGB) with the misorientation angle of 50.5° in a gold nanorod [see HAADF STEM image of another

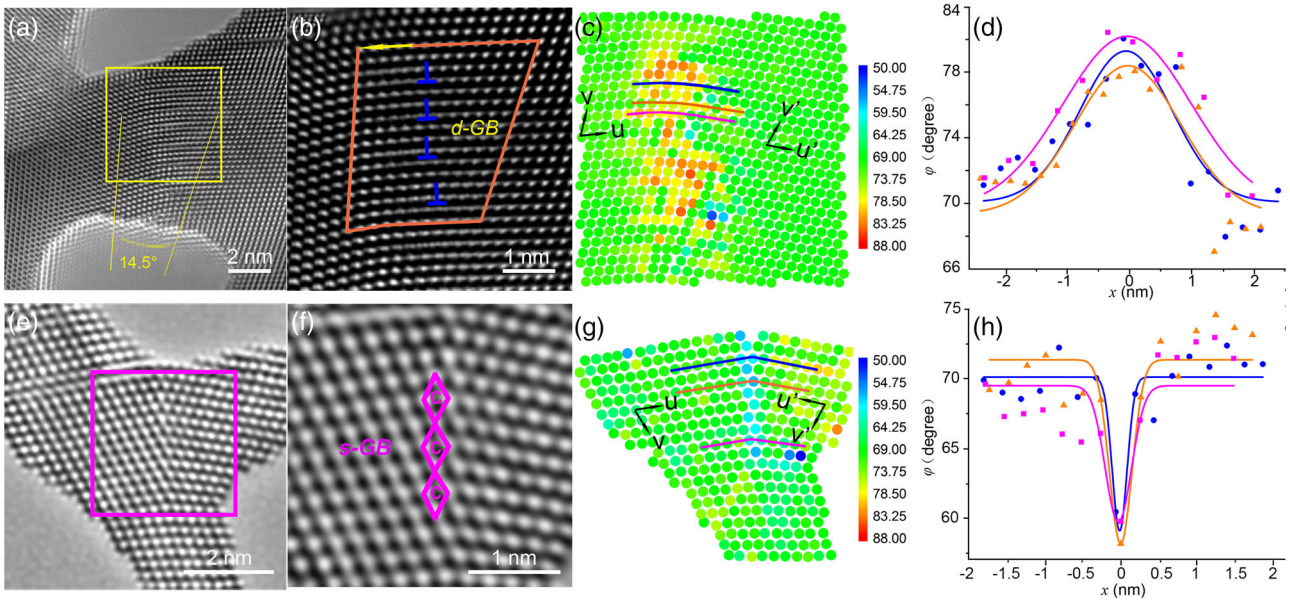

FIG. 2. (a) AC-HRTEM image of a DGB. (b) Enlarged image of the DGB in the yellow-box region in (a). Burgers circuits reveal four dislocations with the same Burgers vector 1/2 [110] in the selected region. (c) Quantitative analysis result from the LADIA program shows the distribution of angle φ between two basic vectors u (or u') and v (or v') across the GB. (d) Line profiles of φ across the DGB along three (111) planes. (e) AC-HRTEM image of a $\Sigma 11(113)$ SGB with the misorientation angle of 50.5°. (f) Enlarged image of the SGB comprised of C-type structural units in the box region in (e). (g),(h) Results show an abrupt change of φ across the SGB.

example of Σ11(113) SGB in Fig. S8 and images of general high-angle GBs as SGBs in Fig. S9 of Ref. [44]]. Figure 2(f) shows the structure of the SGB described by *C*-type structural units [62]. The LADIA results in Figs. 2(g) and 2(h) show an abrupt change of φ, which indicates no obvious elastic strain at the SGB. Comparing the DGB in Fig. 2(a) and the SGB in Fig. 2(e), the width of the DGB (4 nm) is about 8 times that of the SGB (0.5 nm). It also confirms the difference in the strain state (i.e., the existence of an elastic strain field for DGB but not for SGB) between the two types of GBs.

Statistical distribution of two types of GBs with different misorientation angles in nanorods with different diameters is shown in Fig. 3. The GB structures were determined from AC-HRTEM or HAADF STEM investigation. Here, each data point represents a GB with a misorientation angle θ in a nanorod with the diameter of λ. A dividing curve can be drawn according to the data points. Below the curve, GBs exist as dislocation arrays, i.e., DGB type, while above the curve, they exist as structural units, i.e., SGB type. The dividing curve shows an evident size effect in the range of sub-10-nm. When the diameter of a nanorod is larger than 10 nm, the critical misorientation angle approaches 15°, which agrees well with the generally accepted critical angle between low-angle and high-angle GBs in bulk materials [33,34]. However, as the diameter decreases, the critical misorientation angle rises above 15°. When the diameter further decreases to 2 nm, the critical misorientation angle between SGB and DGB increases to 28.6°, which is almost double that for nanorods with diameters larger than 10 nm or in bulk metals. Almost all of the GBs (denoted by solid symbols in Fig. 3) were stable for at least 30 s during the observation. Tilt series of AC-HRTEM images around the [011] zone axis were obtained and analyzed to verify

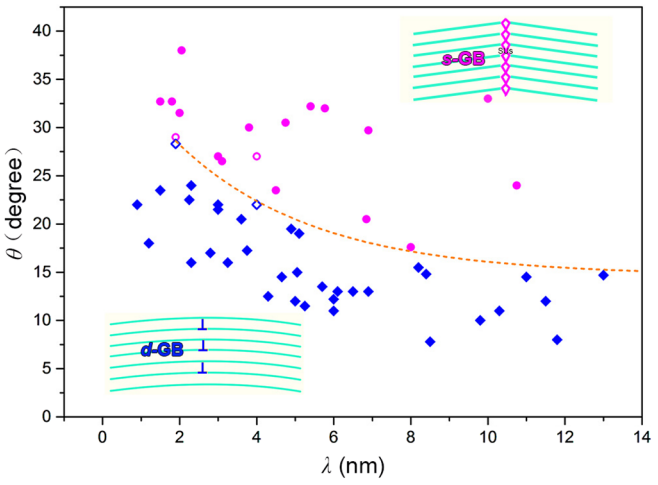

FIG. 3. Statistical distribution of two types of GBs with different misorientation angles θ in gold nanorods with diameters λ. Magenta symbols denote SGBs and blue symbols denote DGBs. All the GBs except those denoted by open symbols are stable for at least 30 s.

the accuracy of the AC-HRTEM imaging for determining the misorientation angle of a GB; see details in Sec. S6 of Ref. [44]. GBs with different misorientation angles in nanorods with different diameters were also measured with the precession electron diffraction technique (see Sec. S7 of Ref. [44]), which shows the same size effect as revealed with the AC-HRTEM method (Fig. 3).

Fluctuation between the DGB and SGB structures was observed in a nanorod as in Figs. 4(a)–4(c) and the unmarked images in Fig. S17 of Ref. [44], when the misorientation angle fluctuated slightly during observation. The GB with the misorientation angle of 28.6° existed as an array of dislocations at the beginning [$t = 0$ s, Fig. 4(a)], then transited to a SGB with the misorientation angle of 29° at 3 s [Fig. 4(b)] but then back to DGB with the misorientation angle of 28.3° at 4.5 s [Fig. 4(c)]. Similar to the GB in Figs. 2(a) and 2(b), a small stress is induced by the asymmetrical nature of the GB in Fig. 4(a), while the strain around the GB is dominated by the dislocations accommodating the misorientation angle (for details, see Sec. S2 of Ref. [44]) During the observation, the diameter and the morphology of the nanorod remained unchanged. This indicates that the electron irradiation effect is negligible under the AC-HRTEM imaging condition (Fig. S20 of Ref. [44]). The result suggests that the critical misorientation angle for a nanorod with the diameter of 2 nm is between 28.6° and 29.0°, and even a small change (<1°) of the misorientation angle around the critical angle would induce the transition of the GB structure. Quantitative analysis by the LADIA program shows the distribution of angle φ in Figs. 4(d)–4(f). Both line profiles [Figs. 4(g) and 4(i)] across the DGBs show a continuously smooth change of φ, while the line profile [Fig. 4(h)] across the SGB shows an abrupt change of φ. Another example (Fig. S21 of Ref. [44]) shows a DGB transited to a SGB during deformation.

Using an *in situ* STM-TEM probe system [Fig. 5(a)], we have measured the electrical resistance change caused by the generation of GBs [Fig. 5(b)] in gold nanorods. Figures 5(c) and 5(d) show that under a bending force applied by the tungsten probe, two GBs were generated in a gold nanorod with a diameter of ∼10 nm. As the GBs formed, an abrupt increase of the electrical resistance by ∼7.5 Ω was detected [Fig. 5(e)]. The misorientation angles of the two GBs are ∼28° and ∼17°, respectively, and the diameter of the nanorod is ∼10 nm. According to the result in Fig. 3, the two GBs are presumably SGBs. The electrical resistance of a SGB is estimated with the formula provided by Miyajima *et al.* [39] with the parameters of the nanorod. The result (for details, see Sec. S12 of Ref. [44]) shows that each SGB in the nanorod corresponds to an electrical resistance increase of ∼2.6 Ω; thus, the two SGBs contribute an increase of ∼5.2 Ω. The rest of the electrical resistance increase is mainly due to the elongation and thinning of the nanorod, which corresponds to an increase

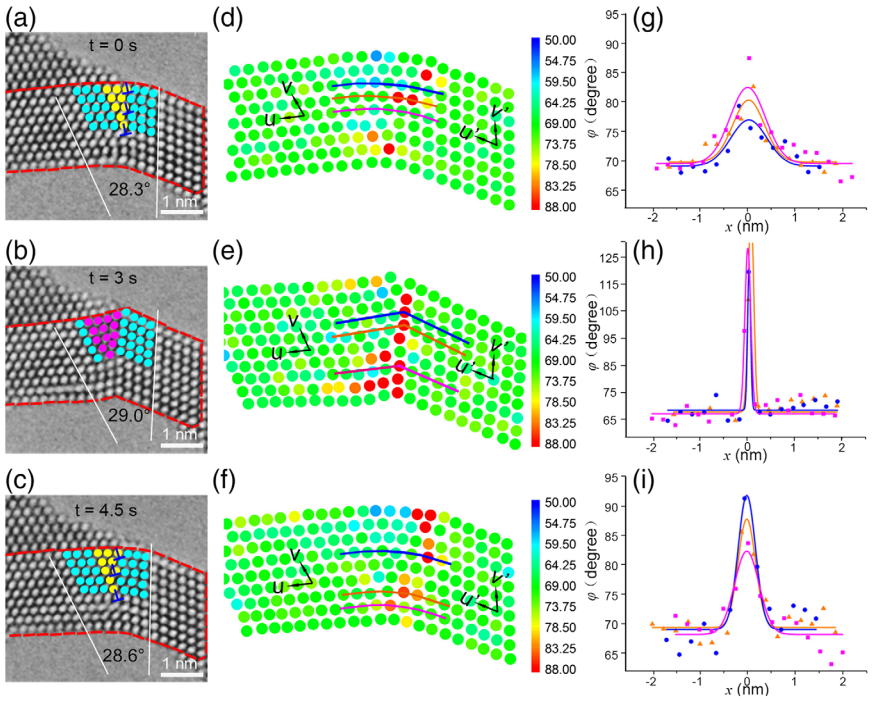

FIG. 4. Structural fluctuation between DGB and SGB in a gold nanorod. (a)–(c) GB structure changes from DGB (a) to SGB (b) and then back to DGB (c). Dislocations of the DGB are marked by blue symbols, while yellow solid circles denote GB atoms of the DGBs. Magenta solid circles denote GB atoms of the SGB and cyan circles denote atoms away from the GBs. (d)–(f) The distribution of φ across the GBs in (a)–(c), respectively. (g)–(i) Line profiles of φ across the GBs in (d)–(f).

of ~2 Ω (for details, see Sec. S12 of Ref. [44]). The above two parts would totally contribute an electrical resistance increase of ~7.2 Ω, matching well with the measured value of ~7.5 Ω. In another nanorod with a diameter of 10 nm, the electrical resistance of the nanorod increased by ~2.3 Ω after a single SGB with the misorientation angle of 27° formed under bending deformation. The measured result also agrees well with the estimated electrical resistance of

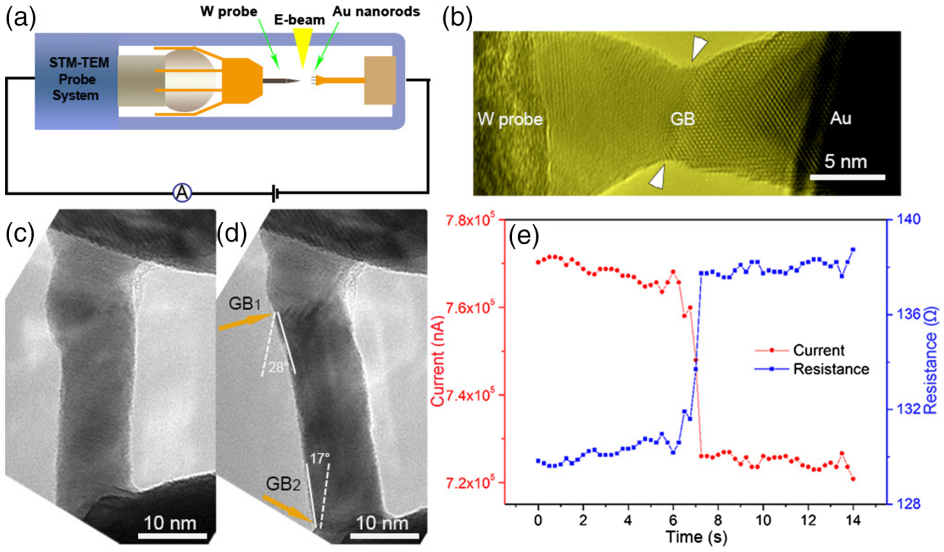

FIG. 5. *In situ* deformation and electrical measurement of a gold nanorod. (a) Experimental setup of a STM-TEM probe system. (b) AC-HRTEM image of a GB formed during *in situ* deformation of a gold nanorod. (c) A gold nanorod with a diameter of 10 nm before bending. (d) Two GBs with the misorientation angles of ~28° and ~17°, respectively, formed during the deformation. (e) Electrical current and resistance of the nanorod before and after the generation of the GBs in (d). The bias voltage applied in the measurement was 100 mV.

2.6 Ω for a SGB (Fig. S22 of Ref. [44]). Meanwhile, the electrical resistance of a nanorod remained almost unchanged when a DGB formed inside (Fig. S23 of Ref. [44]). This indicates that the DGB introduces much less electrical resistance than the SGB.

The substantial elastic strain detected over a broad region around DGBs [e.g., Figs. 2(c) and 2(d)] could be attributed to the small size of the crystals. According to Hirth *et al.* [63,64], only for a DGB in bulk material which can be considered as an infinite dislocation wall and, thus, satisfy the Frank's formula [33], the elastic stress fields of all the component dislocations of the DGB will annihilate each other and, thus, not produce a long-range stress field around the DGB. However, in an ultrathin nanorod, as the DGB ends up at free surfaces in only a few nanometers, the elastic stress field of this finite dislocation wall would exist around the DGB to a considerable extent. On the contrary, GBs comprised of structural units do not produce a long-range stress field; thus, the width of SGBs would be no more than a few atom layers [65], as shown in Figs. 2(g) and 2(h), which is much smaller than that of DGBs. These different GB widths of the two types of GBs can be used to clearly distinguish DGBs from SGBs in our experiments.

According to Koehler [66] and Khannikar *et al.* [67], the elastic energy of a lattice dislocation in a nanorod or nanowire decreases logarithmically when the dislocation approaches the surface [66]. As a result, the total energy of a DGB in a nanorod should be reduced by surface relaxation compared to its counterpart in bulk metals (Fig. S24 of Ref. [44]). For a DGB with a certain misorientation angle, the smaller the diameter of the nanorod, the larger proportion of GB energy would be reduced; hence, GBs in sub-10-nm nanorods with misorientation angles higher than 15° could exist stably as DGBs.

As a DGB is comprised of perfect dislocations, the dislocation arrays should be glissile under a resolved shear stress normal to the boundary plane; that is to say, the DGB should be able to migrate under certain resolved shear stress [68]. On the contrary, SGBs are prone to slide [69,70], which would be fully parallel to the GB and unfortunately result in the breakage of the nanorods. When symmetrical tilt boundaries migrate by a distance D, a shear parallel to the boundary S arises concomitantly, where

$$S/D = 2\tan(\theta/2). \quad (1)$$

Here, θ denotes the misorientation angle [71]. Considering GBs with misorientation angles between 10° and 30°, for example, for a symmetrical GB with a misorientation angle of 15°, the sliding distance S would be only one-fourth of the migration distance D; when θ is 20°, S would be about one-third of D; even when θ reaches 30°, S would be only half of D. Therefore, the shear component parallel to the GB induced by GB migration would be only a fraction of that induced by pure sliding of the SGB in nanorods. In this sense, DGBs instead of SGBs would moderately improve the mechanical stability of sub-10-nm nanorods (for details, see Fig. S25 of Ref. [44]).

Considering the electrical resistivity of a dislocation in metals, the dislocation core rather than the elastic strain field of the dislocation has the major contribution to the electron scattering, as the latter scatters electrons several tens of times weaker than the former [72,73]; that is to say, for a DGB comprised of an array of dislocations, only a portion of atoms, which are in the dislocation cores, of the DGB involved in strongly scattering electrons. However, for a SGB, the structural units scatter electrons as an interfering continuum [74], which means every atom of the SGB would contribute to strong electron scattering. As a result, the electrical resistivity of a SGB would be substantially higher than that of a DGB [35,39,40]. When multiple SGBs formed in a nanorod during deformation (Fig. S26 of Ref. [44]), the induced resistances of the GBs would greatly degrade the electrical conductivity of the nanorod.

The present *in situ* AC-HRTEM investigation on sub-10-nm-sized gold crystals highlights the strong size effect on the GB structure when the diameter of a nanocrystal is smaller than 10 nm. It demonstrates that in sub-10-nm-sized nanorods or nanowires, DGBs instead of SGBs are more likely to form, and this may improve both stabilities of mechanical properties and electrical conductivity of the nanorods or nanowires. Given that applications and research on nano- or molecule devices are developed and deepened and silicon transistors are rapidly approaching dimensions down to sub-10-nm range, this size effect on GB structures could have an important impact on the design of a new generation of nano- or molecular devices.

We thank the National Natural Science Foundation of China (Grants No. 51521091 and No. 51390473) and the Chinese Academy of Sciences (Grant No. QYZDJ-SSW-JSC024) for the financial support. We are grateful to Xuyi Shan, Bo Wu, Chuanbin Jiang, Jingping Cui, and Peng Wu for their help on transmission electron microscopy experiments and sample preparation, and we also thank Miao Song and Lichang Yin for stimulating discussions.

*kuidu@imr.ac.cn

[1] M. Park *et al.*, Nat. Nanotechnol. **7**, 803 (2012).
[2] P. Lee, J. Lee, H. Lee, J. Yeo, S. Hong, K. H. Nam, D. Lee, S. S. Lee, and S. H. Ko, Adv. Mater. **24**, 3326 (2012).
[3] Y. Wu, J. Xiang, C. Yang, W. Lu, and C. M. Lieber, Nature (London) **430**, 61 (2004).
[4] W. Lu and C. M. Lieber, Nat. Mater. **6**, 841 (2007).
[5] L. Hu, H. Wu, and Y. Cui, MRS Bull. **36**, 760 (2011).
[6] N. Liu, M. L. Tang, M. Hentschel, H. Giessen, and A. P. Alivisatos, Nat. Mater. **10**, 631 (2011).
[7] S. Desai *et al.*, Science **354**, 99 (2016).
[8] K. Kordas, G. Toth, P. Moilanen, M. Kumpumaki, J. Vahakangas, A. Uusimaki, R. Vajtai, and P. M. Ajayan, Appl. Phys. Lett. **90**, 123105(2007).

[9] J. D. Meindl, IEEE Micro **23**, 28 (2003).
[10] L. Lu, Y. Shen, X. Chen, L. Qian, and K. Lu, Science **304**, 422 (2004).
[11] C. Wang, Y. Hu, C. M. Lieber, and S. Sun, J. Am. Chem. Soc. **130**, 8902 (2008).
[12] H. Zheng, A. Cao, C. R. Weinberger, J. Y. Huang, K. Du, J. Wang, Y. Ma, Y. Xia, and S. X. Mao, Nat. Commun. **1**, 144 (2010).
[13] J. Wang, F. Sansoz, J. Huang, Y. Liu, S. Sun, Z. Zhang, and S. X. Mao, Nat. Commun. **4**, 1742 (2013).
[14] J. H. Seo *et al.*, Nano Lett. **11**, 3499 (2011).
[15] L. Tian, Y. Q. Cheng, Z. W. Shan, J. Li, C. C. Wang, X. D. Han, J. Sun, and E. Ma, Nat. Commun. **3**, 609 (2012).
[16] D. Jang, X. Li, H. Gao, and J. R. Greer, Nat. Nanotechnol. **7**, 594 (2012).
[17] Z. Zhang, M. M. Mao, J. Wang, B. Gludovatz, Z. Zhang, S. X. Mao, E. P. George, Q. Yu, and R. O. Ritchie, Nat. Commun. **6**, 10143 (2015).
[18] Z. W. Shan, R. K. Mishra, S. A. Syed Asif, O. L. Warren, and A. M. Minor, Nat. Mater. **7**, 115 (2008).
[19] S. Lee, J. Im, Y. Yoo, E. Bitzek, D. Kiener, G. Richter, B. Kim, and S. H. Oh, Nat. Commun. **5**, 3033 (2014).
[20] Q. Yu, Z. W. Shan, J. Li, X. Huang, L. Xiao, J. Sun, and E. Ma, Nature (London) **463**, 335 (2010).
[21] B. Y. Liu *et al.*, Nat. Commun. **5**, 3297 (2014).
[22] S. H. Oh, M. Legros, D. Kiener, and G. Dehm, Nat. Mater. **8**, 95 (2009).
[23] J. Lin *et al.*, Nat. Nanotechnol. **9**, 436 (2014).
[24] B. Wu, A. Heidelberg, and J. J. Boland, Nat. Mater. **4**, 525 (2005).
[25] K. Critchley, B. P. Khanal, M. L. Gorzny, L. Vigderman, S. D. Evans, E. R. Zubarev, and N. A. Kotov, Adv. Mater. **22**, 2338 (2010).
[26] Interface Science and Materials Interconnection, *Proceedings of the Eighth International Conference on Intergranular and Interphase Boundaries in Materials,* edited by M. M. Y. Ishida, T. Suga, H. Ichinose, O. Ohashi, and J. Echigoya (Japan Institute of Metals, Sendai, 1996).
[27] Intergranular and Interphase Boundaries in Materials, *Proceedings of the Seventh International Conference on Intergranular and Interphase Boundaries in Materials*, edited by A. C. Ferro, J. P. Conde, and M. A. Fortes (Trans Tech Publications, Aedermannsdorf, 1995).
[28] M. Tang, W. C. Carter, and R. M. Cannon, Phys. Rev. Lett. **97**, 075502 (2006).
[29] M. L. Bowers, C. Ophus, A. Gautam, F. Lancon, and U. Dahmen, Phys. Rev. Lett. **116**, 106102 (2016).
[30] X. Zhou, N. Tamura, Z. Mi, J. Lei, J. Yan, L. Zhang, W. Deng, F. Ke,B. Yue, and B. Chen, Phys. Rev. Lett. **118**, 096101 (2017).
[31] D. Taha, S. K. Mkhonta, K. R. Elder, and Z. F. Huang, Phys. Rev. Lett. **118**, 255501 (2017).
[32] X. P. Zhang, J. Han, J. J. Plombon, A. P. Sutton, D. J. Srolovitz, and J. J. Boland, Science **357**, 397 (2017).
[33] D. Hull and D. J. Bacon, *Introduction to Dislocations*, 4th ed. (Butterworth-Heinemann, Boston, 2001).
[34] H. Van Swygenhoven, D. Farkas, and A. Caro, Phys. Rev. B **62**, 831 (2000).
[35] T. S. Orlova, A. M. Mavlyutov, A. S. Bondarenko, I. A. Kasatkin, M. Y. Murashkin, and R. Z. Valiev, Philos. Mag. **96**, 2429 (2016).
[36] D. A. Molodov, T. Gorkaya, and G. Gottstein, J. Mater. Sci. **46**, 4318 (2011).
[37] J. Han, V. Vitek, and D. J. Srolovitz, Acta Mater. **133**, 186 (2017).
[38] F. R. N. Nabarro, *Theory of Crystal Dislocations*, International Series of Monographs on Physics (Clarendon Press, Oxford, 1967).
[39] Y. Miyajima, S.-Y. Komatsu, M. Mitsuhara, S. Hata, H. Nakashima, and N. Tsuji, Philos. Mag. **90**, 4475 (2010).
[40] P. Kwapulinski, J. Rasek, and Z. Gierak, Phys. Status Solidi A **107**, 299 (1988).
[41] R. Shao, K. Zheng, Y. Chen, B. Zhang, Q. Deng, L. Jiao, Z. Liao, Z. Zhang, J. Zou, and X. Han, J. Mater. Chem. C **4**, 9303 (2016).
[42] H. J. Jin and J. Weissmuller, Science **332**, 1179 (2011).
[43] X. L. Ye, N. Lu, X. J. Li, K. Du, J. Tan, and H. J. Jin, J. Electrochem. Soc. **161**, C517 (2014).
[44] See Supplemental Material at http://link.aps.org/supplemental/10.1103/PhysRevLett.120.186102 for detailed experimental methods, structural characterization of gold nanorods for electrical measurements and controlled experiments, Figs. S1–S26, and a description of the supplemental video, which includes Refs. [45–58].
[45] Y. Lu, J. Y. Huang, C. Wang, S. Sun, and J. Lou, Nat. Nanotechnol. **5**, 218 (2010).
[46] K. Du and F. Phillipp, J. Microsc. **221**, 63 (2006).
[47] M. J. Hytch, E. Snoeck, and R. Kilaas, Ultramicroscopy **74**, 131 (1998).
[48] C. L. Johnson, E. Snoeck, M. Ezcurdia, B. Rodriguez-Gonzalez, I. Pastoriza-Santos, L. M. Liz-Marzan, and M. J. Hytch, Nat. Mater. **7**, 120 (2008).
[49] M. J. Hytch, J. L. Putaux, and J. M. Penisson, Nature (London) **423**, 270 (2003).
[50] Y. Zhu, C. Ophus, J. Ciston, and H. Wang, Acta Mater. **61**, 5646 (2013).
[51] K. L. Merkle, J. Phys. Chem. Solids **55**, 991 (1994).
[52] K. L. Merkle, Ultramicroscopy **37**, 130 (1991).
[53] Z. Yu, D. A. Muller, and J. Silcox, Ultramicroscopy **108**, 494 (2008).
[54] R. F. Loane, E. J. Kirkland, and J. Silcox, Acta Crystallogr. Sect. A **44**, 912 (1988).
[55] E. F. Rauch, M. Véron, J. Portillo, D. Bultreys, Y. Maniette, and S. Nicolopoulos, Microsc. Anal. **22**, S5 (2008).
[56] Y. Wang, J. He, X. Mu, D. Wang, B. Zhang, Y. Shen, M. Lin, C. Kübel, Y. Huang, and H. Chen, ACS Nano **11**, 5538 (2017).
[57] R. F. Egerton, P. Li, and M. Malac, Micron **35**, 399 (2004).
[58] T. C. Harman, P. J. Taylor, M. P. Walsh, and B. E. LaForge, Science **297**, 2229 (2002).
[59] K. Du, Y. Rau, N. Y. Jin-Phillipp, and F. Phillipp, J. Mater. Sci. Technol. **18**, 135 (2002).
[60] S. J. Wang, H. Wang, K. Du, W. Zhang, M. L. Sui, and S. X. Mao, Nat. Commun. **5**, 3433 (2014).
[61] N. Lu, K. Du, L. Lu, and H. Q. Ye, Nat. Commun. **6**, 7648 (2015).

[62] J. D. Rittner and D. N. Seidman, Phys. Rev. B **54**, 6999 (1996).
[63] J. P. Hirth, D. M. Barkett, and J. Lothe, Philos. Mag. A **40**, 39 (1979).
[64] J. P. Hirth, R. C. Pond, R. G. Hoagland, X. Y. Liu, and J. Wang, Prog. Mater. Sci. **58**, 749 (2013).
[65] G. Gottstein and L. S. Shvindlerman, *Grain Boundary Migration in Metals: Thermodynamics, Kinetics, Applications*, 2nd ed., CRC Series in Materials Science and Technology (Taylor & Francis, Boca Raton, 2010).
[66] J. S. Koehler, Phys. Rev. **60**, 397 (1941).
[67] P. Khanikar, A. Kumar, and A. Subramaniam, Philos. Mag. **91**, 730 (2011).
[68] M. Winning, G. Gottstein, and L. S. Shvindlerman, Acta Mater. **49**, 211 (2001).
[69] Y. H. Zhao, J. F. Bingert, Y. T. Zhu, X. Z. Liao, R. Z. Valiev, Z. Horita, T. G. Langdon, Y. Z. Zhou, and E. J. Lavernia, Appl. Phys. Lett. **92**, 081903 (2008).
[70] M. Y. Gutkin, I. A. Ovid'ko, and N. V. Skiba, J. Phys. D **38**, 3921 (2005).
[71] J. W. Cahn, Y. Mishin, and A. Suzuki, Acta Mater. **54**, 4953 (2006).
[72] D. Trattner, M. Zehetbauer, and V. V. Groger, Phys. Rev. B **31**, 1172 (1985).
[73] A. S. Karolik, J. Phys.: Condens. Matter **13**, 1093 (2001).
[74] R. Dannenberg and A. H. King, J. Appl. Phys. **88**, 2623 (2000).